JOURNAL OF GEOPHYSICAL RESEARCH, VOL. ???, XXXX, DOI:10.1029/,

Equatorial Atlantic interannual variability: the role of heat content

Hui Ding, Noel S Keenlyside, and Mojib Latif

Leibniz Institute of Marine Sciences, Kiel University, Kiel, Germany

Hui Ding, Leibniz Institute of Marine Sciences (IFM-GEOMAR), Düsternbrooker Weg 20, 24105 Kiel, Germany. (hding@ifm-geomar.de)

Abstract.

The dynamics of the Equatorial Atlantic zonal mode are studied using observed sea surface height (SSH), sea surface temperature (SST), and heat flux and reanalysis wind stress and upper ocean temperature. Principal oscillation pattern (POP) analysis shows that the zonal mode is an oscillatory normal-mode of the observed coupled system, obeying the delayed-action/recharge oscillator paradigm for ENSO. Variations in equatorial averaged SSH, a proxy for upper ocean heat content, precede SST anomalies in the cold tongue by 4-5 months, about a quarter of the POP period. Positive subsurface temperature anomalies appear in the west, as a delayed response to the preceding cold event. These propagate eastward, where due to the shallow thermocline they can influence SST, leading to the next warm event. Although SST variations exhibit weak westward propagation during some zonal mode events, POP analysis indicates that to first order there is no zonal propagation in SST. Net surface heat flux anomalies generally act to damp SST anomalies. The zonal mode explains a large amount (70%) of SST variability in the east and a significant fraction (19%) of equatorial variability. Thus, the predictability potential in the Equatorial Atlantic on seasonal time scales may be considerably higher than currently thought.

1. Introduction

The zonal mode [*Xie and Carton*, 2004; *Zebiak*, 1993] dominates interannual climate variability in the Equatorial Atlantic. Zonal mode events primarily peak in boreal summer, but similar variability is also found in November-December [*Okumura and Xie*, 2006]. Associated SST anomalies can exceed 1°C in the Atlantic cold tongue (20°W and 0°W, 6°S and 2°N). Although much weaker than the El Niño Southern Oscillation (ENSO), the zonal mode has major socio-economic impacts, exerting a significant influence on surrounding countries [*Carton and Huang*, 1994], Indian-Summer monsoon [*Kucharski et al.*, 2008; *Wang et al.*, 2009], and possibly also ENSO [*Jansen et al.*, 2009; *Losada et al.*, 2009; *Wang*, 2006; *Wang et al.*, 2009].

The zonal mode's resemblance to ENSO suggests it may arise from similar coupled ocean-atmosphere interaction [*Zebiak*, 1993]. The Bjerknes positive feedback, involving equatorial zonal winds, SST, and upper ocean heat content (HC) is prominent in the structure of peak phase anomalies in observations and reanalysis [e.g., *Ruiz-Barradas et al.*, 2000]. However, each of its three elements explain less variance than in the Pacific [*Keenlyside and Latif*, 2007]. The existence of a delayed negative feedback – necessary for oscillatory behavior – has been investigated less [*Zebiak*, 1993; *Jansen et al.*, 2009]. Intermediate complexity models suggest that HC provides such a feedback and drives phase reversal [*Zebiak*, 1993], as in ENSO [*Jin*, 1997]. In these models, the zonal mode is a normal mode of coupled ocean-atmosphere dynamics [*Wang and Chang*, 2008]. Consistently, Atlantic equatorial averaged HC, from reanalysis and forced ocean model simulations, and observed cold tongue SST variations exhibit a quadrature relationship and are well

fit by the recharge oscillator conceptual model [*Jansen et al.*, 2009]. However, despite similarities to ENSO, significant predictability of the zonal mode has not been shown.

The aim of this paper is to demonstrate that the zonal mode is an oscillatory normal mode of the observed coupled system, and that equatorial HC provides the delayed negative feedback for this mode, and hence a basis for seasonal prediction in the Equatorial Atlantic. We use both SSH and thermocline (20° isotherm) depth as proxies for upper ocean HC; all three quantities are closely related in the equatorial region, because of the two-layered nature of the tropical oceans. The paper is organized as follows. Section 2 gives a brief introduction to POP analysis and describes the data used. The oscillatory mechanisms of the equatorial Atlantic zonal mode are investigated in section 3 using primarily observations for the period 1993 to 2008. In section 4 these results are corroborated by repeating the analysis over a longer period (1958-2001) using data from an ocean model simulation. Conclusions and discussions are given in section 5.

2. Method and data

POP analysis [*Von Storch et al.*, 1988] is a linearized form of the more general Principal Interaction Pattern (PIP) analysis [*Hasselmann*, 1988] and used here to identify the normal modes of Equatorial Atlantic interannual climate variability. It is a method for extracting the eigenmodes of variability in multidimensional data. The POPs (or Empirical Normal Modes [*Penland and Sardeshmukh*, 1995]) are the eigenvectors of the system matrix A obtained by fitting the data to a multivariate first-order Markov process $\vec{X}(t+1) = A\vec{X}(t) + n$, where $A = C_1 C_0^{-1}$ with C_1 and C_0 denoting the lag +1 and lag 0 covariance matrices of $\vec{X}(t)$, and n a white noise forcing.

In general, POPs are complex with real and imaginary parts $\vec{P}^1$ and $\vec{P}^2$. They can describe traveling modes or standing waves. The complex eigenvalues define a rotation period and an e-folding time for exponential decay. The time evolution $Z_1(t)$ and $Z_2(t)$ of the POPs are obtained from the projection of the original time series on the adjoint POPs. If the two coefficient time series are in quadrature, as theoretically expected, the evolution of the system in the two-dimensional POP space can be understand as a cyclic sequence of patterns: $\cdots \longrightarrow \vec{P}^2 \longrightarrow \vec{P}^1 \longrightarrow -\vec{P}^2 \longrightarrow -\vec{P}^1 \longrightarrow \cdots$.

After having identified a certain POP, it is often desirable to describe the signal in terms of other simultaneously observed variables $\vec{v}(t)$. Here, this is done with the "associated correlation pattern", denoted by $\vec{P}_v^1$ and $\vec{P}_v^2$. These can be obtained by minimizing $[\|\vec{v}(t) - \frac{Z_1(t)}{\sigma^1}\vec{P}_v^1 - \frac{Z_2(t)}{\sigma^2}\vec{P}_v^2\|]$. Here, $\|\|$ denotes a quadratic norm. The time coefficients $Z_1(t)$ and $Z_2(t)$ of the identified POP are normalized by their own standard deviation σ^1 and σ^2, respectively so that the patterns $\vec{P}_v^1$ and $\vec{P}_v^2$ have the same unit as variable $\vec{v}(t)$.

Here, two separate POP analysis are performed. The first covers the period 1993 to 2008 and uses satellite measurements of SSH (AVISO, http://www.aviso.oceanobs.com/) and SST (OISST, *Reynolds et al.* [2002]), and wind stress from the NCEP/NCAR reanalysis [*Kalnay et al.*, 1996]. The second covers the period 1958-2001 and uses observed reconstructed SST (HadISST, *Rayner et al.* [2003]), NCEP/NCAR reanalysis wind stress, and 20^{o}C isotherm depths from a NCEP/NCAR reanalysis forced ocean model [*Marsland et al.*, 2003] simulation. In the ocean model, standard bulk formulas for the calculation of heat fluxes and a weak relaxation of surface salinity to climatological observations [*Levitus and Boyer*, 1994] are used. Data from the simulation were used in previous studies

of equatorial Atlantic variability [*Keenlyside and Latif*, 2007; *Jansen et al.*, 2009], where results were carefully checked using various other observations and reanalysis.

The domain analysed in this study is 45°W to 5°E and 10°S to 10°N, as we focus on the equatorial zonal mode. However, our results are not sensitive to the exact choice of east-west domain (not shown). Prior to POP analysis, data were detrended and band-pass filtered to retain variations with periods between 8 and 80 months, and all quantities are normalized with their mean field standard deviation. The POP analysis uses the first six empirical orthogonal functions (EOFs), capturing 69.3% (68.1%) of the total variance for 1993-2008 (1958-2001) analysis. However, explained variance is always computed with respect to the raw monthly mean data. POP analysis using more than six EOFs reveals very similar results (not shown).

3. Results: 1993–2008

POP analysis of monthly SSH, SST, and wind stress reveals one dominant complex POP (Fig. 1a-d). It accounts for 19% of the total (unfiltered) variance, and considerably more locally: up to 40% in eastern Atlantic SSH (Fig. 2a), 70% in cold tongue SST (Fig. 2b), and 30% in South Atlantic surface zonal wind (Fig. 2c), but is low for meridional wind (Fig. 2d). This POP has a rotation period of 19 months, which is evident in the time evolution coefficients (Fig. 1e), and an e-folding time of 36 months. The period was corroborated by cross spectral analysis (not shown), which provides a robuster estimate [*Xu and Von Storch*, 1990]. It is shorter than other estimates from observations [30 months; *Latif and Grötzner*, 2000; *Ruiz-Barradas et al.*, 2000], theory [3 years; *Wang and Chang*, 2008], and intermediate complexity models [4 years; *Zebiak*, 1993]. This may reflect non-

stationary behavior in the frequency of the zonal mode, given the different time intervals considered. All other POPs are not relevant to the zonal mode phenomenon.

The real POP component (Fig. 1b,d) is associated with the zonal mode's peak warm phase. It is consistent with the structure obtained from rotated-EOF analysis [*Ruiz-Barradas et al.*, 2000] and with an active Bjerknes feedback [*Keenlyside and Latif*, 2007]. SST anomalies in the eastern Equatorial Atlantic (Fig. 1d) are accompanied by anomalous northwesterly surface winds to the west (Fig. 1d). Maximum negative SSH anomalies occur in the western Atlantic on both sides of the equator, while in the east there are strong positive anomalies at the equator; the pattern is reminiscent of Rossby and Kelvin wave structures. The imaginary POP component (Fig. 1a,c) corresponds to the transition phase, a quarter of the rotation period prior to the peak. At this time a significant SSH signal has appeared in the equatorial wave guide (Fig. 1a), reflecting a build up of the HC. SST anomalies, however, are relatively weak (Fig. 1c) compared to those of the real component (Fig. 1d). Therefore, zonal mode SST variability can be regarded to first order as a standing oscillation (i.e., exhibiting no zonal propagation), although hovmoeller diagram of both raw and POP reconstructed SST anomalies (not shown) show weak westward propagation in some events. This is in contrast to *Wang and Chang* [2008], as SST anomalies in their theoretical mode migrate rapidly westward during the growth phase. In addition, in their mode SST variability extends to the northwestern Atlantic, while in our's it is constrained to the cold tongue. The zonal mode is argued to be a mixed SST-thermocline depth mode [*Zebiak*, 1993]. However, results here suggest the delayed-action/recharge oscillator mechanisms may dominate (consistent with *Jansen*

et al. [2009]), given that heat content variations are important (Fig. 1a, b) and SST fluctuations exhibit a standing pattern (Fig. 1c, d).

Interestingly, the POP mode also shows evidence of a northwesterly surface wind anomalies in the South Atlantic. These correspond to a relaxation of southeasterly Trades during the transition from the imaginary to real pop phases, and are consistent with development of warm anomalies there. Similar features are identified by composite and rotated-EOF analyses, which suggest an interaction among equatorial and Angola/Benguela SST variations and the South Atlantic anti-cyclone [*Hu and Huang*, 2007; *Lübbecke et al.*, accepted]. These studies indicate that the zonal mode is not a pure equatorial phenomenon, and that off-equatorial variations may be important in triggering the zonal mode.

The relevance of the recharge oscillator paradigm [*Jin*, 1997] in the Atlantic is further assessed by investigating the relationship between equatorial averaged HC (using SSH and thermocline depth as proxies) and cold tongue SST. SSH variations tend to lead SST variations, displaying a maximum correlation of 0.47 when SSH leads SST by about two months (Fig. 3). Data from the NCEP ocean reanalysis supports this relation, with equatorial averaged thermocline depth variations leading SST, with a maximum correlation (0.4) when thermocline depth variations lead by three months (Fig. 3). Different from SSH, thermocline depth and SST variations are in near quadrature with an almost zero simultaneous correlation. Forced ocean model simulations give similar results, with boreal summer equatorial averaged thermocline depth and autumn SST most strongly related [*Jansen et al.*, 2009]. The POP reconstruction exhibits a similar relationship, but it is stronger, and SSH and SST variations are less in quadrature (Fig. 3). It also indicates that equatorial averaged SSH acts as a delayed negative feedback for the zonal mode,

as a strong anticorrelation (-0.6) occurs when SST variations lead SSH fluctuations by 6 months (Fig. 3). This phase relationship is in accord with model results [*Zebiak*, 1993] and the delayed action/recharge oscillator mechanism [*Jansen et al.*, 2009].

It is useful to compare these results with those of the Pacific, where a similar relationship exists [*Meinen and McPhaden*, 2000]. There the maximum correlation (in raw data) is 0.77 when equatorial SSH anomalies lead Niño3 SST variations by 3 months (not shown). Thus, although upper ocean HC (as estimated by SSH and thermocline depth) provides memory for SST variability in the Atlantic on seasonal timescales, it is much less than in the Pacific. However, the relationship in the Atlantic might be underestimated in raw data, as fresh water perturbations to SSH in the west under the intertropical convergence zone may mask the dynamical signal and spoil the HC/SST quadrature relationship [*Schouten et al.*, 2005; *Ding et al.*, 2009]. The analysis of ocean model data below somewhat supports this notion.

The recharge/discharge of equatorial HC, achieved by equatorial waves, is evident in the vertical structure of equatorial upper ocean temperature during different phases of the zonal mode (Fig. 4). During the transition to the warm phase there is a build up of equatorial heat content, expressed in a basin wide deepening of the thermocline that causes weak warm SST anomalies in the cold tongue (Fig. 4a). The positive Bjerknes feedback amplifies these anomalies and leads to the peak warm phase, with significant deepening of the thermocline in the east and strong SST anomalies at the surface (Fig. 4b). Discharge of equatorial HC has already begun at this time (Fig. 3), and cold subsurface temperature anomalies are intruding into the equatorial wave guide in the west (Fig. 4b). The latter accumulate and propagate eastward causing basin wide negative anomalies

in the thermocline (i.e., the negative of Fig. 4a), which in turn lead to cooling in the cold tongue and the negative phase of the zonal mode. These subsurface temperature changes are reminiscent of those in the Pacific, providing further support for the delayed action/recharge oscillator mechanism in the Atlantic.

Analysis above indicates that interannual variability in Equatorial Atlantic SST results mainly from ocean dynamics. This is supported by the simultaneous anticorrelation (-0.46) between net surface heat flux and SST averaged over the cold tongue (Fig. 3); this is consistent with previous studies that found that surface heat flux variations damp SST anomalies in the eastern South Atlantic near the Gulf of Guinea [*Hu and Huang*, 2006, 2007]. Although net surface heat flux mainly damps SST variability, it can sometimes help drive SST changes, for example following strong El Niño events [*Chang et al.*, 2006] and in the western tropical Atlantic [*Hu and Huang*, 2006, 2007]; surface heat flux variations may also be important in driving SST anomalies on shorter time scales. The complexity of the upper ocean heat budget adds difficulty to seasonal prediction of Equatorial Atlantic variability [*Chang et al.*, 2006].

4. Results: 1958–2001

The POP analysis of SST, 20^oC isotherm depth, and surface wind stress for the period 1958-2001 reveals one dominant complex POP (Fig. 5), accounting for 20% of the total (unfiltered) variance. This POP has a rotation period of 30 months (confirmed by cross spectral analysis) and an e-folding time of 26 months. The period is longer than that found above, but consistent with other estimates from observations [30 months; *Latif and Grötzner*, 2000; *Ruiz-Barradas et al.*, 2000]. No other POPs are relevant here.

The POP patterns (Fig. 5) bear strong resemblance to those obtained from data for the shorter period (Fig. 1), with one main difference: during the transition phase heat content anomalies of same sign extend along the whole of the equator (Fig. 5a); this is more consistent with the delayed-action/recharge oscillator mechanisms. Another difference is that compared to Fig. 1d, the SST anomaly pattern in Fig. 5d is less focused on the equator and may have a stronger projection onto the meridional mode [*Ruiz-Barradas et al.*, 2000; *Wang and Chang*, 2008]. Local explained variances (Fig. 6a) in thermocline depth also display a more consistent structure with equatorial Rossby and Kelvin waves than in SSH (Fig. 2a). This is consistent with fresh water perturbations masking the dynamical signal in sea level under the ITCZ in the western tropical Atlantic [*Schouten et al.*, 2005; *Ding et al.*, 2009]. Correlation between simulated thermocline depth and observed SSH from 1993 to 2001 (not shown) is low (0.2) in those areas where explained variances in SSH is low (less than 10%) but higher (over 0.4) in regions of high explained variance in SSH. Local explained variances in SST, zonal and meridional wind stress display some difference, possibly due to the different time interval analyzed. These data also support the relationship between equatorial heat content and cold tongue SST (Fig. 7), but it is somewhat weaker than in the SSH and SST above (Fig. 3) (possible reasons for this are described in the next section). The subsurface temperature patterns during transition and mature phase are also very similar to those above (not shown). These results therefore support the mechanisms presented by POP analysis of relatively short data.

5. Conclusions and discussion

The zonal mode is identified as a normal mode of observed Equatorial Atlantic interannual variability, through POP analysis of essentially observational data between 1993-

2008. During this interval, it explains 19% of the total variance and has a period of 19 months. The zonal mode is dominated by delayed action/recharge oscillator mechanism, where HC (as measured by SSH and thermocline depth) provides memory, and thus a basis for seasonal prediction. This work supports previous studies based on intermediate complexity [*Zebiak*, 1993], and conceptual models [*Jansen et al.*, 2009], and provides further evidence for the role of HC in Equatorial Atlantic variability. POP analysis of longer data sets (1958-2001) corroborates the mechanism proposed here, despite identifying a different oscillation period (30 months). Previous studies (e.g., *Zebiak* [1993]; *Frankignoul and Kestenare* [2005]; *Illig and Dewitte* [2006]; *Wang and Chang* [2008]) indicate that the zonal mode is stable, and that external/stochastic forcing is required to sustain it. The oscillatory character revealed by POP method does not contradict these studies. Furthermore, POP analysis cannot directly address the stability of the zonal mode, as it is a linear analysis.

The shorter period found in the analysis of data from 1993 to 2008 may reflect non-stationarity in the frequency of zonal mode, but it could also be due to the short length of data. POP analysis of the sub-periods 1956-1970, 1971-1985 and 1986-2000 identifies dominant periods of 28, 23 and 22 months, respectively. Although this is consistent with non-stationarity, sensitivity to data length cannot be completely excluded, as all three periods are shorter than 30 months. The literature also reports quite different estimates for the dominant period of the zonal mode (e.g., 30 months [*Latif and Grötzner*, 2000; *Ruiz-Barradas et al.*, 2000], 4 years [*Zebiak*, 1993; *Jansen et al.*, 2009]), but all are longer than 19-months. Estimated periods are generally not equal to an integral number years, despite the strong seasonality of the zonal mode [*Xie and Carton*, 2004]. Thus, the

interaction with the annual cycle is a further complication in estimating the zonal mode's period. Longer high-quality data are required to resolve these issues.

The variance explained by the zonal mode is locally large and up to 70% in cold tongue SST (Fig. 2b). Given the importance of this mode for precipitation in surrounding countries, it is important to be able to predict it to the extent possible. The level of predictability may be estimated from the oscillatory nature of the POP. The maximum lagged-linear correlation between the imaginary component time series and cold tongue SST (r=0.55; Fig. 1e) suggests around 30% (r=0.55) of cold tongue SST variability could be predicted at 4-months lead. And around 80% (r=0.9) at 2-months lead, implied by the relationship with equatorial averaged heat content POP (Fig. 3). These values are consistent with estimates based on fitted conceptual models [*Jansen et al.*, 2009]. Nevertheless they are based on a highly simplified picture and higher values may be achievable using complex dynamical models, and in particular seasons and for specific events [*Kleeman and Moore*, 1999].

The direct relationship between equatorial averaged SSH and cold tongue SST (Fig. 3) implies much lower skill, reflecting that equatorial averaged SSH and the imaginary POP are poorly related (Fig. 1a). This may be because SSH is not an ideal proxy for HC, as in the NCEP ocean reanalysis (not shown) and forced ocean model simulations (Fig. 5), equatorial averaged thermocline depth and the imaginary POP are closely related. However, the relationship between equatorial heat content and cold tongue SST remains weak in these products (Fig. 3 & 7). But differences among these products are not small, due to model deficiencies, sparse ocean data for assimilating, and inaccurate surface forcing.

Alternatively, the recharge oscillator mechanisms may explain much less variance than suggested by the POP analysis or other dynamics may better describe equatorial Atlantic variability. In particular, complex remote forcing from ENSO [*Chang et al.*, 2006] might contribute to mask the HC signal. Also, unlike in the Pacific, the Atlantic equatorial cold tongue is centered south of the equator and how equatorial waves influence this region may be different. Other possible mechanisms include, the western Pacific oscillator [Weisberg and Wang, 1997], advective-reflective oscillator [Picaut et al., 1997; Wang, 2001], or a destabilized basin mode [*Jin and Neelin*, 1993; *Keenlyside et al.*, 2007]. The western Pacific oscillator, however, is probably not active in the Atlantic, as no negative SST or westward wind stress anomalies exist in the western Atlantic during the zonal mode's peak phase (Fig 1b). Zonal current variations are important in both the advective-reflective oscillator and destabilized basin-mode mechanisms. Preliminary analysis of zonal currents, model and satellite-derived, suggest a possible role for the basin mode (not shown). However, explained variances are substantially smaller than that for heat content (SSH and thermocline depth). Further analysis and better ocean heat content data are required to resolve these issues.

Results here offer some promise for seasonal prediction in the Atlantic. However, two things are required before useful skill might be realised. First, the major systematic errors of complex models [*Davey et al.*, 2002; *Richter and Xie*, 2008; *Wahl et al.*, 2009] in simulating the equatorial Atlantic climate need to be reduced. In most models these errors are so large that they inhibit feedbacks necessary for interannual variability. Second, better observations of upper ocean heat content in the Equatorial Atlantic are required to accu-

rately initialised forecasts. We hope that this work should further stimulate developments in these two areas.

Acknowledgments. The work was supported by the German BMBF NORDATLANTIK project and the SFB 754 of DFG. POP calculations were performed at the Rechenzentrum der Univerität Kiel. NSK is funded by the DFG Emmy Noether Programme. Figures were created using Ferret, a product of NOAA's Pacific Marine Environmental Laboratory.

References

Carton, J., and B. Huang (1994), Warm Events in the Tropical Atlantic, *J. Phys. Oceanogr.*, *24*(5), 888–903, doi:10.1175/1520-0485(1994)024<0888:WEITTA>2.0.CO;2.

Chang, P., Y. Fang, R. Saravanan, L. Ji, and H. Seidel (2006), The cause of the fragile relationship between the Pacific El Niño and the Atlantic Niño., *Nature*, *443*(7109), 324, doi:10.1038/nature05053.

Davey, M., et al. (2002), STOIC: a study of coupled model climatology and variability in tropical ocean regions, *Climate Dyn.*, *18*(5), 403–420, doi:10.1007/s00382-001-0188-6.

Ding, H., N. Keenlyside, and M. Latif (2009), Seasonal cycle in the upper equatorial Atlantic Ocean, *J. Geophys. Res.*, *114*(C9), C09,016, doi:10.1029/2009JC005418.

Frankignoul, C., and E. Kestenare (2005), Air-sea interactions in the tropical Atlantic: a view based on lagged rotated maximum covariance analysis, *J. Climate*, *18*(18), 3874–3890, doi:10.1175/JCLI3498.1.

Hasselmann, K. (1988), PIPs and POPs: The Reduction of Complex Dynamical Systems Using Principal Interaction and Oscillation Patterns, *J. Geophys. Res.*, *93*(D9), 11,015–11,021, doi:10.1029/JD093iD09p11015.

Hu, Z., and B. Huang (2006), Physical processes associated with the tropical Atlantic SST meridional gradient, *J. Climate*, *19*(21), 5500–5518, doi:10.1175/JCLI3923.1.

Hu, Z., and B. Huang (2007), Physical processes associated with the tropical Atlantic SST gradient during the anomalous evolution in the southeastern ocean, *J. Climate*, *20*(14), 3366–3378, doi:10.1175/JCLI4189.1.

Illig, S., and B. Dewitte (2006), Local coupled equatorial variability versus remote ENSO forcing in an intermediate coupled model of the tropical Atlantic, *J. Climate*, *19*(20), 5227–5252, doi:10.1175/JCLI3922.1.

Jansen, M., D. Dommenget, and N. Keenlyside (2009), Tropical atmosphere–ocean interactions in a conceptual framework, *J. Climate*, *22*(3), 550–567, doi:10.1175/2008JCLI2243.1.

Jin, F. (1997), An Equatorial Ocean Recharge Paradigm for ENSO. Part I: Conceptual Model, *J. Atmos. Sci.*, *54*(7), 811–829, doi:10.1175/1520-0469(1997)054<0811:AEORPF>2.0.CO;2.

Jin, F., and J. Neelin (1993), Modes of interannual tropical ocean-atmosphere interaction-a unified view. Part I: Numerical results, *J. Atmos. Sci.*, *50*(21), 3477–3477, doi:10.1175/1520-0469(1993)050<3477:MOITOI>2.0.CO;2.

Kalnay, E., et al. (1996), The NCEP/NCAR 40-Year Reanalysis Project, *Bull. Am. Meteorol. Soc.*, *77*(3), 437–471, doi:10.1175/1520-0477(1996)077<0437:TNYRP>2.0.CO;2.

Keenlyside, N., and M. Latif (2007), Understanding Equatorial Atlantic Interannual Variability, *J. Climate*, *20*(1), 131–142, doi:10.1175/JCLI3992.1.

Keenlyside, N., M. Latif, and A. Durkop (2007), On Sub-ENSO Variability, *J. Climate*, *20*(14), 3452–3469, doi:10.1175/JCLI4199.1.

Kleeman, R., and A. Moore (1999), A new method for determining the reliability of dynamical ENSO predictions, *Mon. Wea. Rev.*, *127*(5), 694–705, doi:10.1175/1520-0493(1999)127<0694:ANMFDT>2.0.CO;2.

Kucharski, F., A. Bracco, J. H. Yoo, and F. Molteni (2008), Atlantic forced component of the Indian monsoon interannual variability, *Geophys. Res. Lett.*, *35*, 4706–+, doi:10.1029/2007GL033037.

Latif, M., and A. Grötzner (2000), The equatorial Atlantic oscillation and its response to ENSO, *Climate Dyn.*, *16*(2), 213–218, doi:10.1007/s003820050014.

Levitus, S., and T. Boyer (1994), World Ocean Atlas, *Washington DC: NOAA*, *1*, 117.

Losada, T., B. Rodríguez-Fonseca, I. Polo, S. Janicot, S. Gervois, F. Chauvin, and P. Ruti (2009), Tropical response to the Atlantic Equatorial mode: AGCM multimodel approach, *Climate Dyn.*, *33*(1), 1–8, doi:10.1007/s00382-009-0624-6.

Lübbecke, J., C. Böning, N. Keenlyside, and S.-P. Xie (accepted), On the connection between Benguela and Equatorial Atlantic Niños and the role of the South Atlantic Anticyclone.

Marsland, S., H. Haak, J. Jungclaus, M. Latif, and F. Roske (2003), The Max-Planck-Institute global ocean/sea ice model with orthogonal curvilinear coordinates, *Ocean Model.*, *5*(2), 91–127, doi:10.1016/S1463-5003(02)00015-X.

Meinen, C., and M. McPhaden (2000), Observations of warm water volume changes in the equatorial Pacific and their relationship to El Niño and La Niña, *J. Climate*, *13*(20), 3551–3559, doi:10.1175/1520-0442(2000)013<3551:OOWWVC>2.0.CO;2.

Okumura, Y., and S. Xie (2006), Some Overlooked Features of Tropical Atlantic Climate Leading to a New Niño-Like Phenomenon*, *J. Climate*, *19*(22), doi: 10.1175/JCLI3928.1.

Penland, C., and P. D. Sardeshmukh (1995), The optimal growth of tropical sea surface temperature anomalies, *J. Climate*, *8*(8), 1999–2024, doi:10.1175/1520-0442(1995)008<1999:TOGOTS>2.0.CO;2.

Rayner, N., D. Parker, E. Horton, C. Folland, L. Alexander, D. Rowell, E. Kent, and A. Kaplan (2003), Global analyses of sea surface temperature, sea ice, and night marine air temperature since the late nineteenth century, *J. Geophys. Res.*, *108*(D14), 4407–4453, doi:10.1029/2002JD002670.

Reynolds, R., N. Rayner, T. Smith, D. Stokes, and W. Wang (2002), An Improved In Situ and Satellite SST Analysis for Climate, *J. Climate*, *15*(13), 1609–1625, doi: 10.1175/1520-0442(2002)015<1609:AIISAS>2.0.CO;2.

Richter, I., and S. Xie (2008), On the origin of equatorial Atlantic biases in coupled general circulation models, *Climate Dyn.*, *31*(5), 587–598, doi:10.1007/s00382-008-0364-z.

Ruiz-Barradas, A., J. Carton, and S. Nigam (2000), Structure of interannual-to-decadal climate variability in the tropical Atlantic sector, *J. Climate*, *13*(18), 3285–3297, doi: 10.1175/1520-0442(2000)013<3285:SOITDC>2.0.CO;2.

Schouten, M., R. Matano, and T. Strub (2005), A description of the seasonal cycle of the equatorial Atlantic from altimeter data, *Deep-Sea Res.*, *52*(3), 477–493, doi:

10.1016/j.dsr.2004.10.007.

Von Storch, H., T. Bruns, I. Fischer-Bruns, and K. Hasselmann (1988), Principal Oscillation Pattern Analysis of the 30-to 60-Day Oscillation in General Circulation Model Equatorial Troposphere, *J. Geophys. Res.*, *93*(D9), 11,022–11,036, doi: 10.1029/JD093iD09p11022.

Wahl, S., M. Latif, W. Park, and N. Keenlyside (2009), On the Tropical Atlantic SST warm bias in the Kiel Climate Model, *Climate Dyn.*, *33*(6), 174, doi:10.1007/s00382-009-0690-9.

Wang, C. (2006), An overlooked feature of tropical climate: Inter-Pacific-Atlantic variability, *Geophys. Res. Lett.*, *33*(12), L12,702, doi:10.1029/2006GL026324.

Wang, C., F. Kucharski, R. Barimalala, and A. Bracco (2009), Teleconnections of the tropical Atlantic to the tropical Indian and Pacific Oceans: A review of recent findings, *Meteorologische Zeitschrift*, *18*(4), 445–454, doi:10.1127/0941-2948/2009/0394.

Wang, F., and P. Chang (2008), A Linear Stability Analysis of Coupled Tropical Atlantic Variability, *J. Climate*, *21*(11), 2421–2436, doi:10.1175/2007JCLI2035.1.

Xie, S., and J. Carton (2004), Tropical Atlantic variability: Patterns, mechanisms, and impacts, *Earth's Climate: The Ocean-Atmosphere Interaction, Geophys. Monogr*, *147*, 121–142.

Xu, J., and H. Von Storch (1990), Predicting the State of the Southern Oscillation Using Principal Oscillation Pattern Analysis, *J. Climate*, *3*(12), 1316–1329, doi:10.1175/1520-0442(1990)003<1316:PTSOTS>2.0.CO;2.

Yu, L., and R. Weller (2007), Objectively Analyzed air-sea heat Fluxes (OAFlux) for the global oceans, *Bull. Am. Meteorol. Soc.*, *88*, 527–539, doi:10.1175/BAMS-88-4-527.

Zebiak, S. (1993), Air–Sea Interaction in the Equatorial Atlantic Region, *J. Climate*, *6*(8), 1567–1586, doi:10.1175/1520-0442(1993)006<1567:AIITEA>2.0.CO;2.

Figure 1. (a, b) SSH and (c, d) SST and wind stress from the dominant POP mode, (left) imaginary and (right) real components and (e) their corresponding time series and SST averaged over 20°W and 0°W, 6°S and 2°N (box in d). The maximum correlation between cold tongue SST and the real (imaginary) POP component time series is 0.89 (0.55) at zero-lag (when SST lags by 4-5 months). Real and imaginary components are most strongly related (r=0.7) when the imaginary component leads by 4-5 months.

Figure 2. Local explained variances are computed using the dominant POP mode (Fig. 1) and with respect to raw monthly mean anomalies of (a) SSH, (b) SST, and (c) zonal and (d) meridional surface wind stress.

Figure 3. Cross-correlation between Equatorial Atlantic (3°S-3°N) averaged SSH and cold tongue averaged SST computed from the dominant POP mode, corresponding raw monthly mean data, and also using thermocline depth from NCEP reanalysis (http://www.esrl.noaa.gov/psd/) instead of SSH. Cross-correlation between cold tongue SST and net surface heat flux [*Yu and Weller*, 2007] is also shown. Period considered is 1993-2008.

Figure 4. Associated correlation pattern in subsurface temperature anomalies along the equator during the (a) transition and (b) peak phases of the zonal mode, as respectively obtained by linear regression of imaginary and real POP time coefficients (Fig. 1) on to NCEP reanalysis ocean temperature.

.

Figure 5. (a, b) 20^oC isotherm depth (Z20) and (c, d) SST and wind stress from the dominant POP mode, (left) imaginary and (right) real components. This figure corresponds to Fig. 1, but 20^oC isotherm depth from a forced ocean model simulation are used instead of SSH, and the period 1958-2001 is considered.

Figure 6. Local explained variances are computed using the dominant POP mode (Fig. 5) and with respect to raw monthly mean anomalies of (a) 20^oC isotherm depth (Z20), (b) SST, and (c) zonal and (d) meridional surface wind stress. This figure corresponds to Fig. 2, but 20^oC isotherm depth from a forced ocean model simulation are used instead of SSH, and the period 1958-2001 is considered.

Figure 7. Cross-correlation between Equatorial Atlantic (3°S-3°N) averaged 20^oC isotherm depth (Z20) and cold tongue averaged SST computed from the dominant POP mode and corresponding raw monthly mean data. This figure corresponds to Fig. 3, but 20^oC isotherm depth from a forced ocean model simulation are used instead of SSH, and the period 1958-2001 is considered.

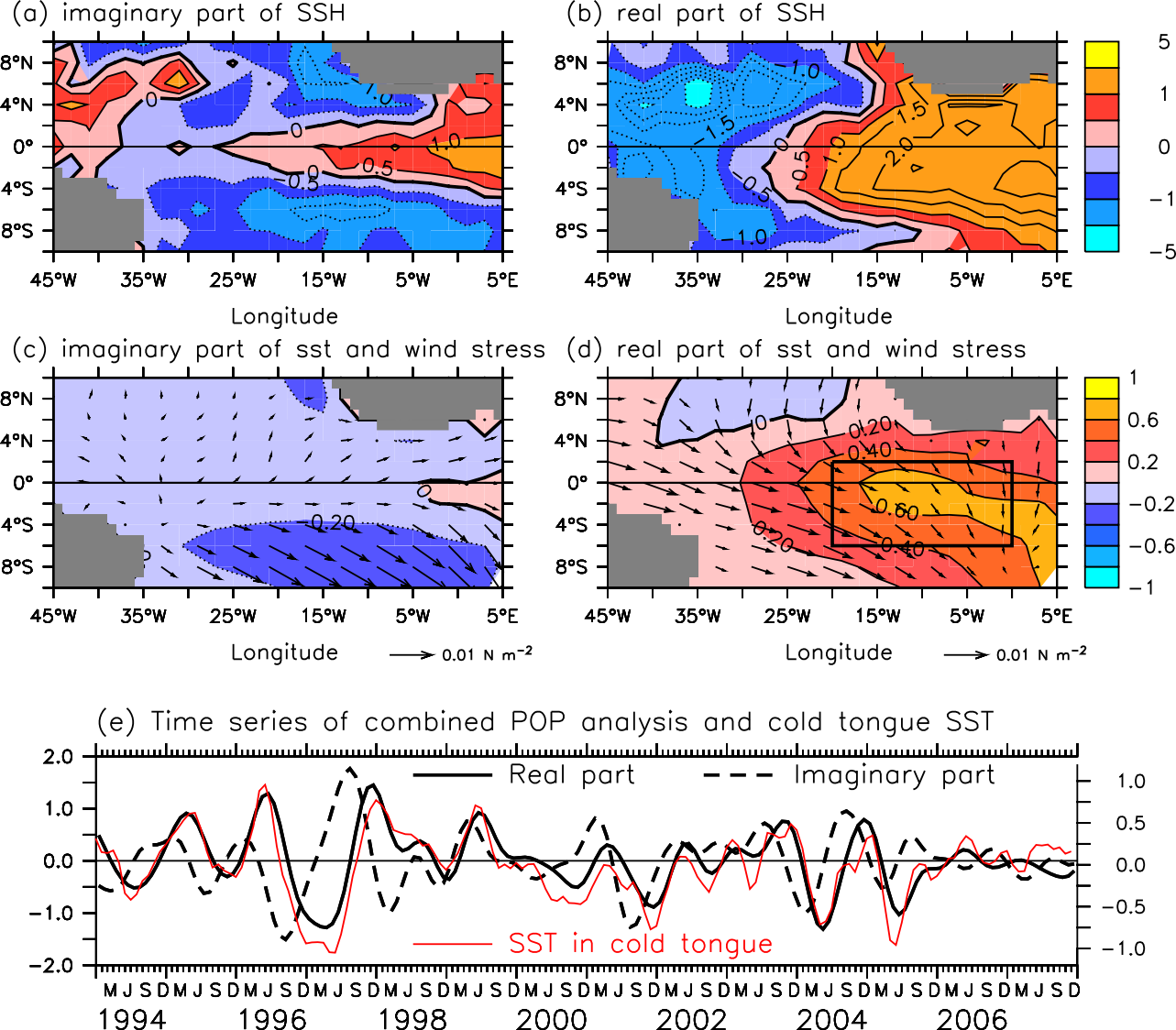
(a) imaginary part of SSH
(b) real part of SSH
(c) imaginary part of sst and wind stress
(d) real part of sst and wind stress
8°N
4°N
0°
4°S
8°S
45°W
35°W
25°W
15°W
5°W
5°E
Longitude
0.01 N m⁻²
(e) Time series of combined POP analysis and cold tongue SST
Real part
Imaginary part
SST in cold tongue
M J S D M J S D M J S D M J S D M J S D M J S D M J S D M J S D M J S D M J S D M J S D M J S D M J S D
1994
1996
1998
2000
2002
2004
2006

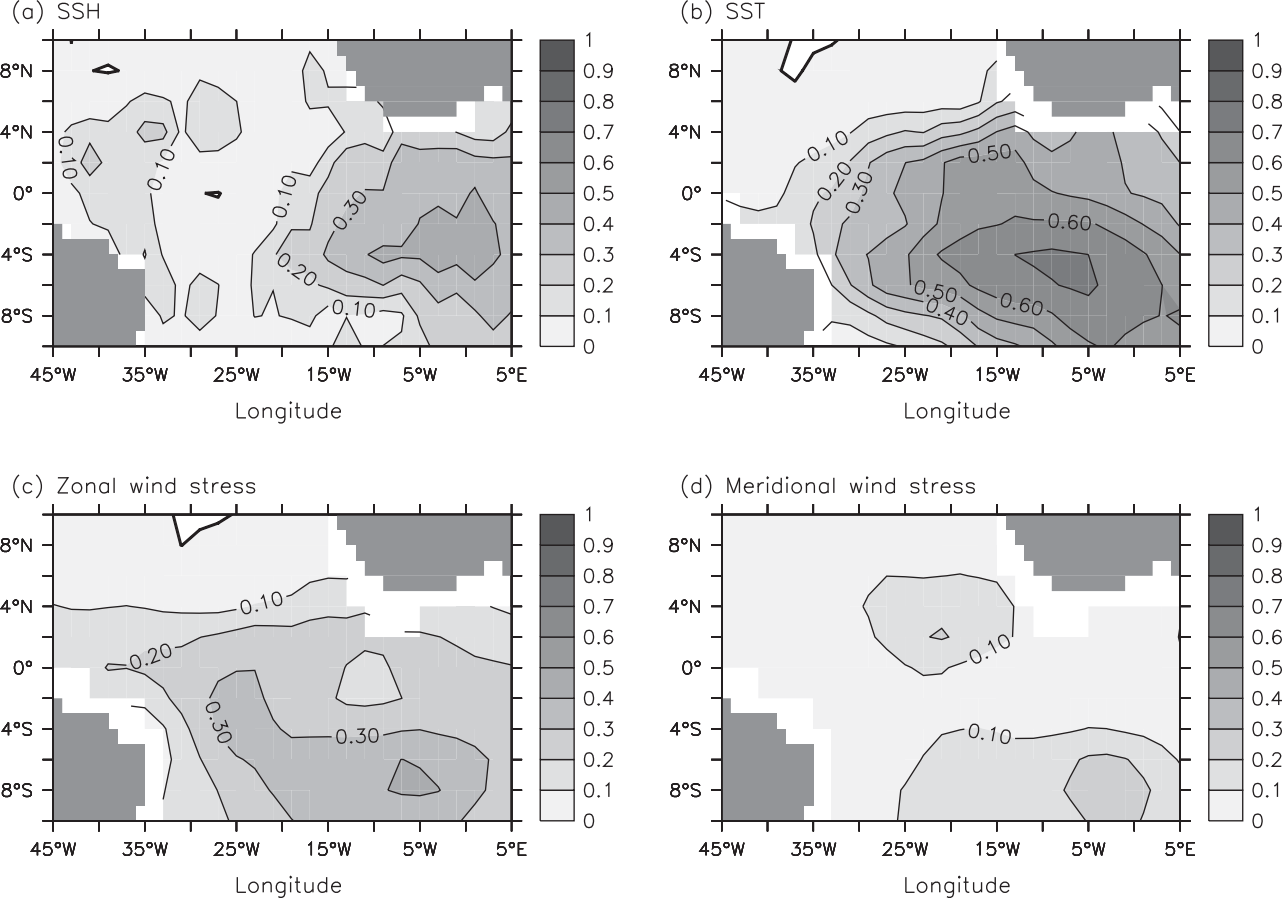
(a) SSH
(b) SST
(c) Zonal wind stress
(d) Meridional wind stress
8°N
4°N
0°
4°S
8°S
45°W
35°W
25°W
15°W
5°W
5°E
Longitude
0.10
0.20
0.30
0.40
0.50
0.60
1
0.9
0.8
0.7
0.6
0.5
0.4
0.3
0.2
0.1
0

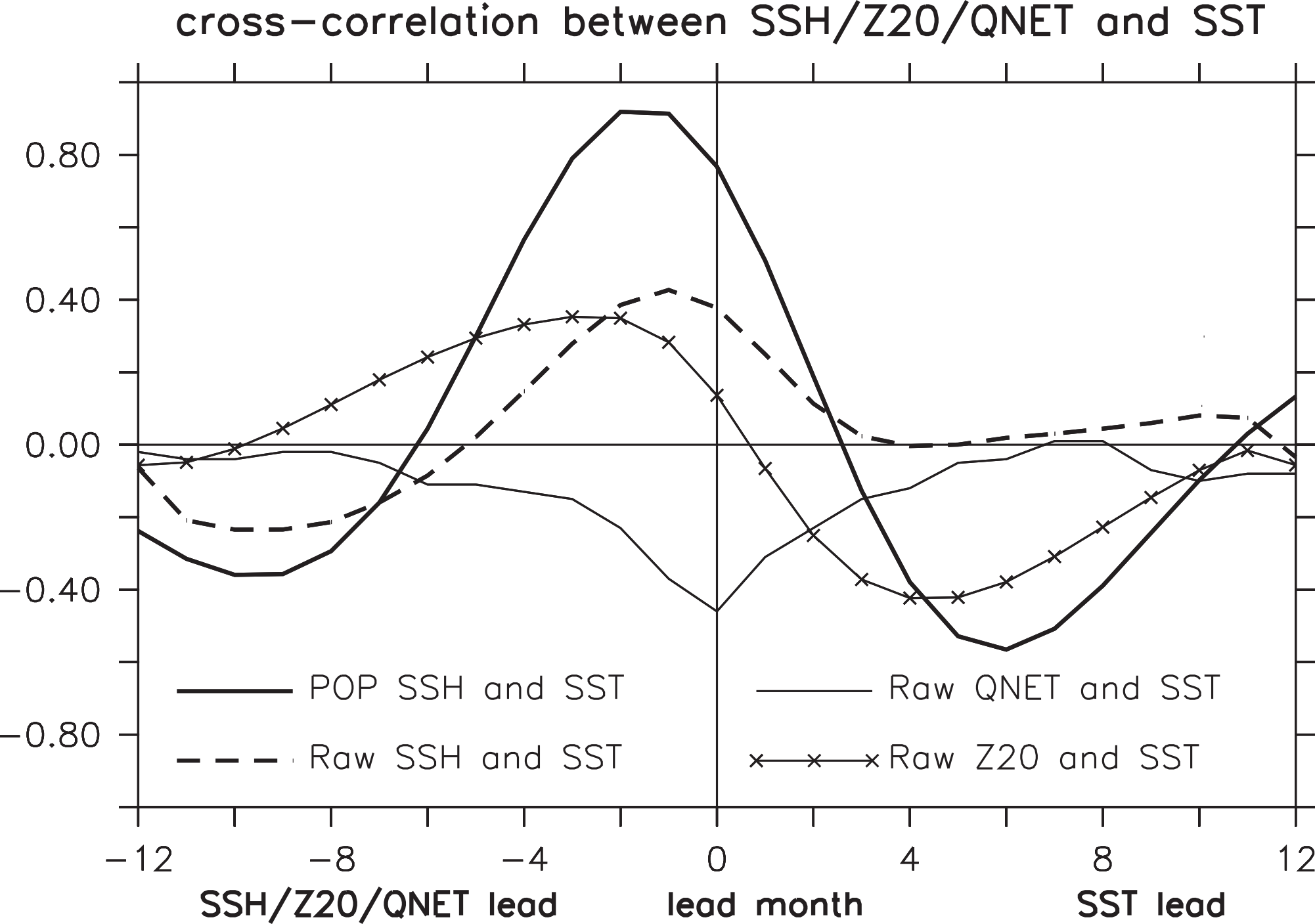
cross−correlation between SSH/Z20/QNET and SST
0.80
0.40
0.00
−0.40
−0.80
POP SSH and SST
Raw SSH and SST
Raw QNET and SST
Raw Z20 and SST
−12
−8
−4
0
4
8
12
SSH/Z20/QNET lead
lead month
SST lead

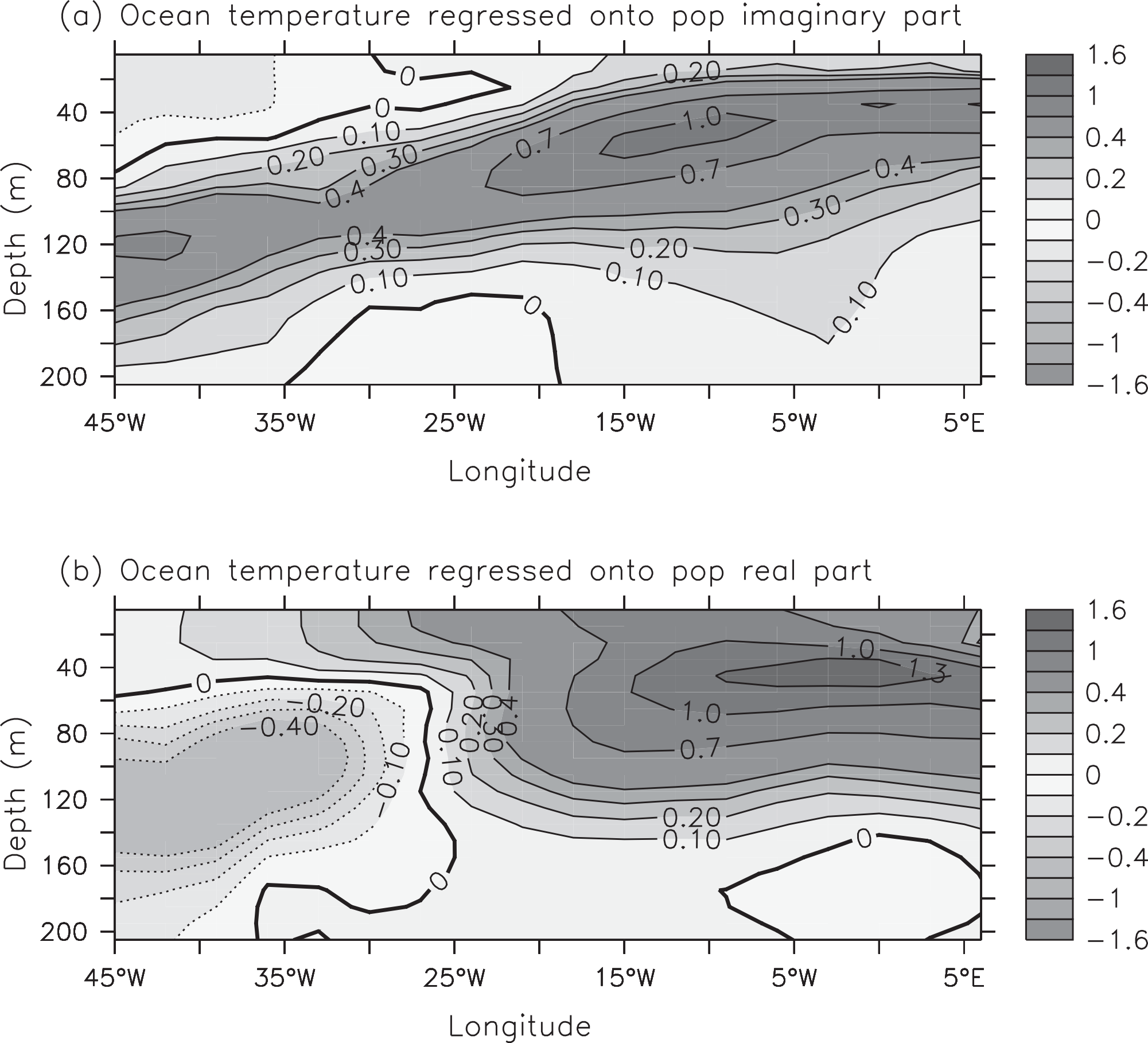
(a) Ocean temperature regressed onto pop imaginary part
Depth (m)
40
80
120
160
200
45°W
35°W
25°W
15°W
5°W
5°E
Longitude
0
0.20
0
0.10
0.20
0.30
0.4
1.0
0.7
0.7
0.4
0.30
0.4
0.30
0.20
0.10
0.10
0
0.10
1.6
1
0.4
0.2
0
−0.2
−0.4
−1
−1.6
(b) Ocean temperature regressed onto pop real part
Depth (m)
40
80
120
160
200
45°W
35°W
25°W
15°W
5°W
5°E
Longitude
0
−0.20
−0.40
−0.10
0.10
0.20
0.40
0
1.0
1.3
1.0
0.7
0.20
0.10
0
1.6
1
0.4
0.2
0
−0.2
−0.4
−1
−1.6

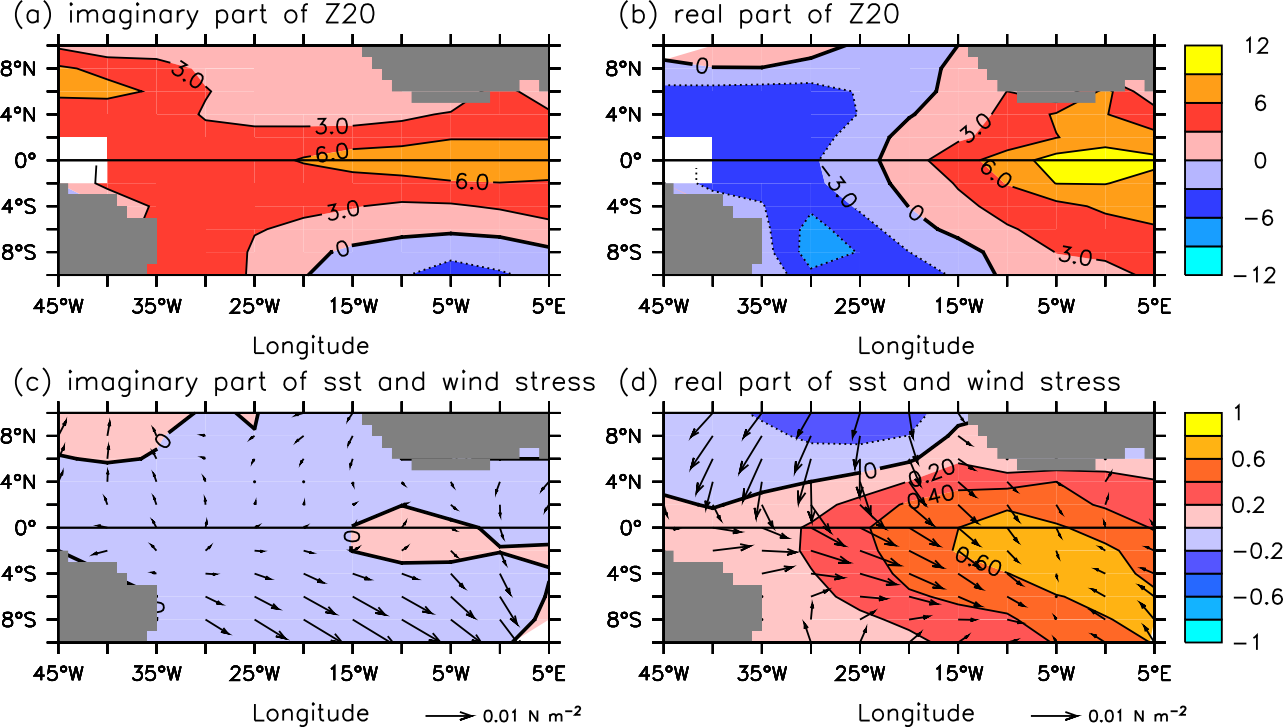
(a) imaginary part of Z20
(b) real part of Z20
(c) imaginary part of sst and wind stress
(d) real part of sst and wind stress
8°N
4°N
0°
4°S
8°S
45°W
35°W
25°W
15°W
5°W
5°E
Longitude
3.0
6.0
0
−3.0
0.20
0.40
0.60
12
6
0
−6
−12
1
0.6
0.2
−0.2
−0.6
−1
0.01 N m⁻²

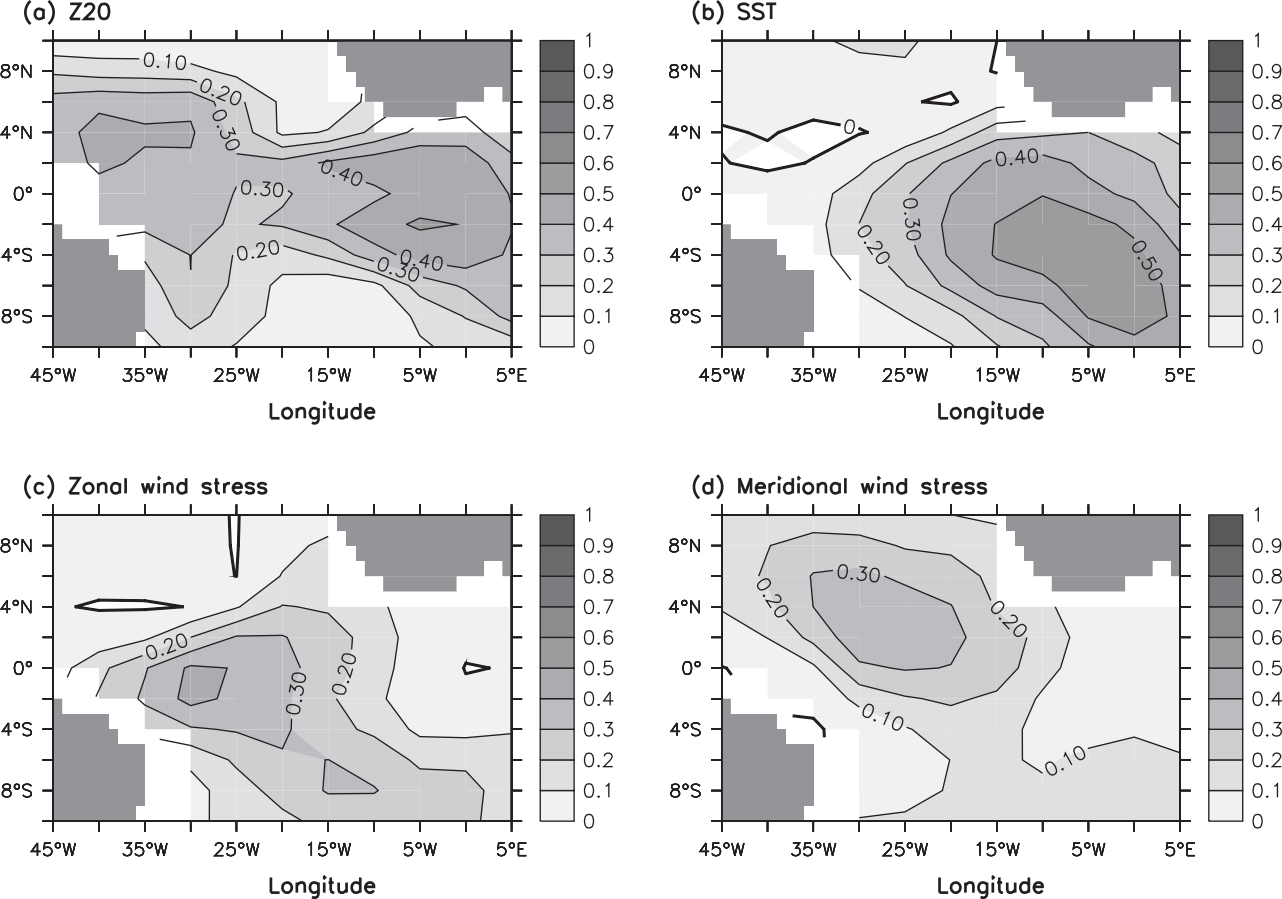
(a) Z20
0.10
0.20
0.30
0.40
0.30
0.20
0.40
0.30
(b) SST
0
0.40
0.30
0.20
0.50
(c) Zonal wind stress
0.20
0.30
0.20
(d) Meridional wind stress
0.30
0.20
0.20
0.10
0.10
8°N
4°N
0°
4°S
8°S
45°W
35°W
25°W
15°W
5°W
5°E
Longitude
1
0.9
0.8
0.7
0.6
0.5
0.4
0.3
0.2
0.1
0

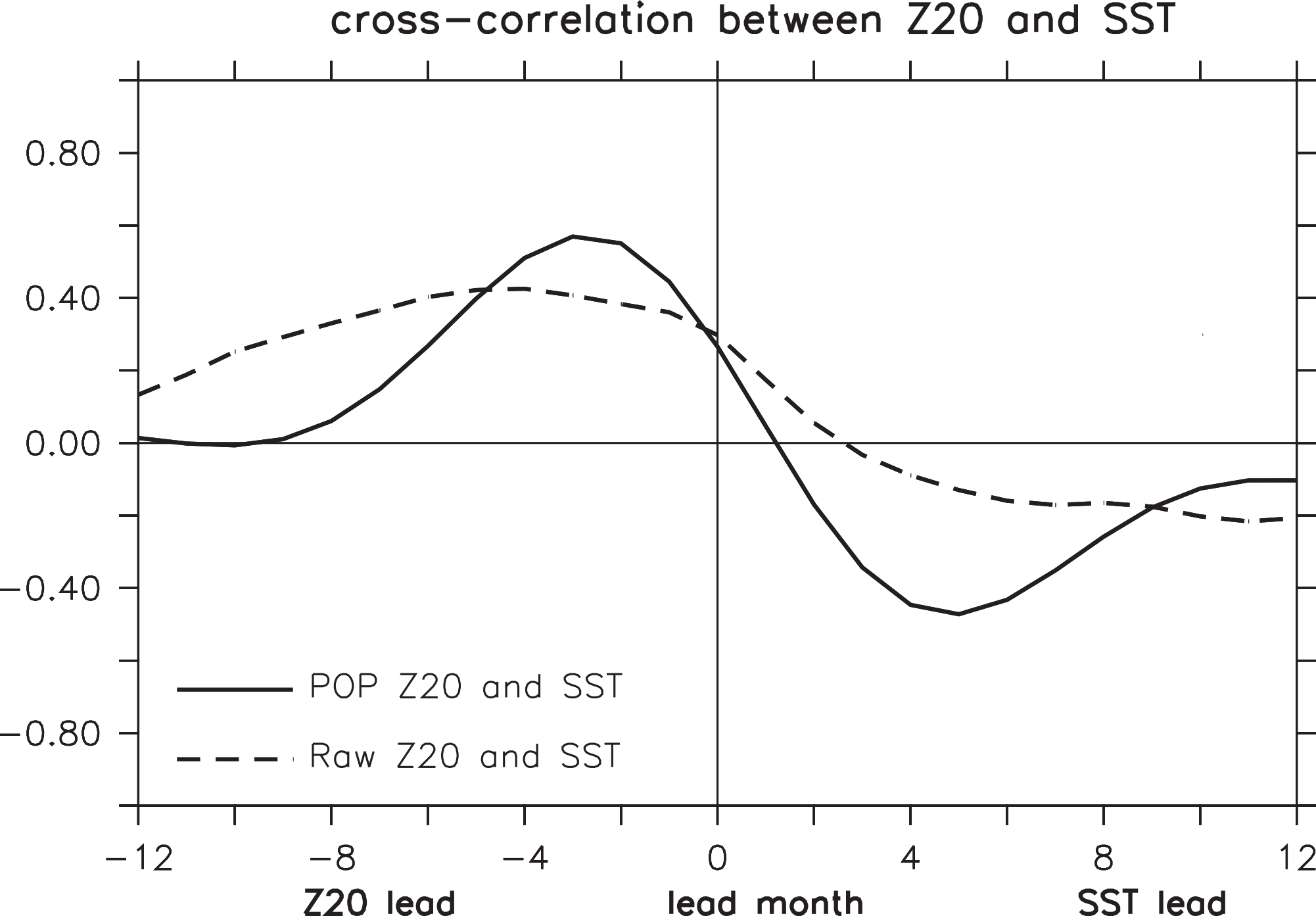
cross−correlation between Z20 and SST
0.80
0.40
0.00
−0.40
−0.80
POP Z20 and SST
Raw Z20 and SST
−12
−8
−4
0
4
8
12
Z20 lead
lead month
SST lead